Synthesis of optically important transparent SnS$_2$/PS composites films through chemical route and their photocatalytic applications

R. Mohapatra[a,b], J. B. Kaundal[a,b], Y. C. Goswami[a,b,*]
[a]Nano research lab, Department of Physics, School of Sciences
ITM University, Gwalior, India
[b]SoS in Physics Jiwaji University Gwalior, India

Optically important SnS$_2$/Polystyrene (PS) transparent flexible composites were synthesized by low cost sol gel route and characterized using structural, morphological, and optical analysis. Polystyrene exhibits amorphous nature however an excellent improvement in crystallization is observed on inclusion of fresh developed SnS$_2$ in polystyrene. FTIR peaks were also confirms the formation of SnS$_2$/PS composites. AFM micrographs shows spheres like structures in morphology and this tendency increases with increase in sulfur ratio to tin. The increment in roughness of the composites is also observed with increase in sulfur ratio. The composites exhibits excellent photocatalytic activity with about 97% methyl Red dye degradation presence of sunlight.

1. Introduction

The chalcogenides always have a huge attraction by researchers due to their excellent absorption properties in the visible region. This property is been utilized for the last two decades in solar cells [1], photovoltaic cells [2, 3], supercapacitors, and lithium-ion batteries [4]. Recently the nano form of chalcogenides has also shown a lot of potential in tuning various optical properties and hence, increased inefficient use of the solar light spectrum [5-7]. The research on SnS nanoparticles is relatively new and have lot of future application due to its low toxicity in comparison to other chalcogenides. SnS$_2$ is an II-VI semiconductor material and has a narrow band range. It has 1.38 eV direct bandgap and 1.09 eV indirect bands [8]. The low bandwidth and low toxicity of SnS$_2$ nanoparticles make it useful in many future applications such as the development of biomedical, optoelectronic devices [9-10], photocatalysts [11-13], and gas detection devices [14]. The morphology of particles strongly depends upon the preparation method. The size and shape of the nanoparticles are dependent on the synthesis process. SnS have different phases like SnS, Sn2S, Sn2S3, and S3nS4 [15-18]. SnS$_2$ can also be useful in composite form with polymers with increased functionality. The present work is based on SnS$_2$/Polystyrene (PS), which is a type of heat cooler used in the packaging of electrical appliances [19-20]. PS is widely used in the packaging of food materials, and other appliances because of their good thermal and impermeable properties. However, after use in packaging, it produces huge amounts of waste and pollutants to the environment. Many researchers have reported the ways to recycle of polystyrene with various methods: by adding some metal oxide, chalcogenides nanoparticles in it and synthesizing new composites called polymer nanocomposites [18-23]. In our present work, we've synthesized SnS$_2$/PS nanocomposites in two stages. In the first stage, SnS nanoparticles were obtained by using the sol-gel method and in the second stage, transparent SnS$_2$/PS

---

nanocomposites were grown as self-sustained layers and as layers on glass substrates. The nanocomposites show excellent photodegradation of methyl red dye, which indicates how waste material can be used to obtain composites as having great potential for dye degradation

2. Experimental details

2.1. Materials

All chemicals used were of analytical grade and used as received without any further purification. All Tin (II) chloride dehydrate (99.9%) $SnCl_2 \cdot 2H_2O$, Thiourea (NH_2CSNH_2), Toluene, Acetone and Ethanol were purchased from Aldrich. whatsman filter paper No. 042 was used for the filtration. Thermocol waste was collected and washed with distilled water and dried at room temperature.

2.2. Synthesis of tin sulfide and SnS/PS

Low-cost Sol –Gel method is used for the synthesis of Tin sulfide nanoparticles and films. 0.1M Tin chloride $SnCl2 \cdot 2H2O$ and 0.1M Thiourea were used as starting precursors. Double distilled water was used for dissolving the precursors. Initially, 0.76g of thiourea was dissolved in 100ml of distilled water and the solution was continuously stirred for 30 minutes. In the next step, 2.63g $SnCl2 \cdot 2H2O$ was added and further stirred for another 30min. A few drops of liquid ammonia were added and finally, the sol was left for stirring for about 3h. This solution is irradiated by microwave for 5min and after this continues stirring was done at room temperature. The samples were prepared with various sulfur concentrations, (a) Sample C1: 1g thiourea, (b) 2.268g of thiourea C2 (c) 3.8g of thiourea C3. In the last step solution of Polystyrene, the solution is added in a sample and polymer-based flexible films were obtained on the glass as well as self-sustaining position.

The reaction of $SnCl4.2H2O$ with thiourea produced H2S. Then SnS2 nanoparticles were obtained via the reaction of Sn+4 with H2S. The process could be as follows:

$$H_2NCSNH_2 + 2H_2O \rightarrow CO_2 + 2NH_3 + H_2S,$$
$$Sn^{+4} + 2H_2S \rightarrow SnS_2 + 4H^+.$$
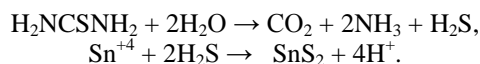
2.3. Materials Characterization

Films and particles were obtained and characterized by structural, Morphological and optical characterizations. X-ray diffractograms were obtained in the angle of 2theta ranging from 2^0 to 80^0. Nickel foil is used as filter in the instrument to select the Cu kα radiation of wavelength 1.5413 A^0 from the copper source using Bruker D8 Advanced XRD. Flexible film is cut into 1x1cm piece which is used to as sample. AFM micrographs were obtained by using digital Instrumentation-Inc, USA. By conducting mode, at UGC-DAE consortium research Centre Indore. PL and UV-Vis spectra were carried by Perkin Elmer Lambda-25 and Perkin Elmer LS-55. Fourier- transform infrared (FTIR) spectra were obtained by Perkin Elmer Spectrum 2 using KBr pellets in the range (500-4000 cm-1). Materials and chemical bond were identified and analyzed by FTIR Spectra.

2.4. Photocatalytic experiments

The SnS_2/PS nanocomposites were used for photocatalytic activity studies of methyl Red dye under sunlight. All the photocatalytic reactions in the present study were carried out under direct sunlight between 12:00 noon and 14:00 pm. In experiment. The beaker was kept under sunlight for irradiation, and solutions were withdrawn at periodic time intervals and centrifuged. The solutions were analyzed using a UV−Vis spectrophotometer (Perkin Elmer Lambda 25). The catalytic experiments were carried out under similar conditions using SnS_2/PS nanocomposites. The degradation efficiency of Methyl Red was calculated using the formula given below.

$$\% \text{ Degradation percentage} = \left(\frac{A0-A}{A0}\right) \times 100\%$$

where A_o is the concentration of Methyl Red at time is zero and its adsorption equilibrium and A is the concentration of Methyl Red at different illumination times of sunlight. To understand the mechanism of photo degradation of Methyl Red better, and to prove the involvement of hydroxyl radicals in the photo degradation in the presence of SnS/PS as the catalyst was used as a probe molecule [23-30]

3. Results and discussion

3.1. Structural Studies (X-Ray diffraction)

X- Ray diffractograms of SnS_2/PS nanocomposites are obtained and shown in Fig 1a. All the peaks are identified for SnS_2 structures with JCPDS card no.22-0951, however one or two peaks for SnS are also observed. The intensities of the reflections are very small. The samples were A matching of the observed and standard (*hkl*) planes confirmed that the samples are of SnS_2 having a hexagonal structure. All of the peaks in the XRD pattern can be readily indexed to a pure hexagonal phase of SnS_2 with a lattice constant a=3.649 Å and c=5.899 Å, which are in good agreement with the literature values (JCPDS card no. 22–0951). In Fig3a.The dominant peak is 100 is broad indicates the particles are in nano range. However increase in the size observed with increasing SnS_2 ratio. Debey-Scherrer formula is being deployed to find the average size of the particles [1] that is in nano range and has been shown in Table 1 where crystallite size broadening is β_t and β_ε is the strain induced broadening, and β_{hkl} is the FWHM of instrumental corrected The observed XRD line broadening is due to crystallite size and strain contribution featured by the Williamson–Hall (W–H) plots and can be written as

$$D = {0.9\lambda}/{\beta Cos\theta} \quad \dots\dots Eq(1) \dots\dots\dots\dots [29]$$

$$\beta_{hkl} = \beta_t + \beta_\varepsilon$$

Broadening. Eq. 2 is obtained by considering both the broadenings and represents the uniform deformation model (UDM) where the isotropic nature of the crystal is considered, which means the material properties are independent of the direction in which they have measured. The model is shown in Figure 3b.

$$\beta_{hkl} cos\theta = \frac{K\lambda}{D} + 4\varepsilon \sin\theta_{hkl} \quad\quad\quad (Eq. 2)$$

The estimated size and strain have been tabulated in Table 1. The positive slope for samples implies the presence of tensile strain. It has been attributed to lattice distortion. Due to strain the numbers of peaks decrease in SnS/PS[30]. In first sample C1 large numbers of peaks are present the quantity is sulfur increases the peaks are decreasing in number.
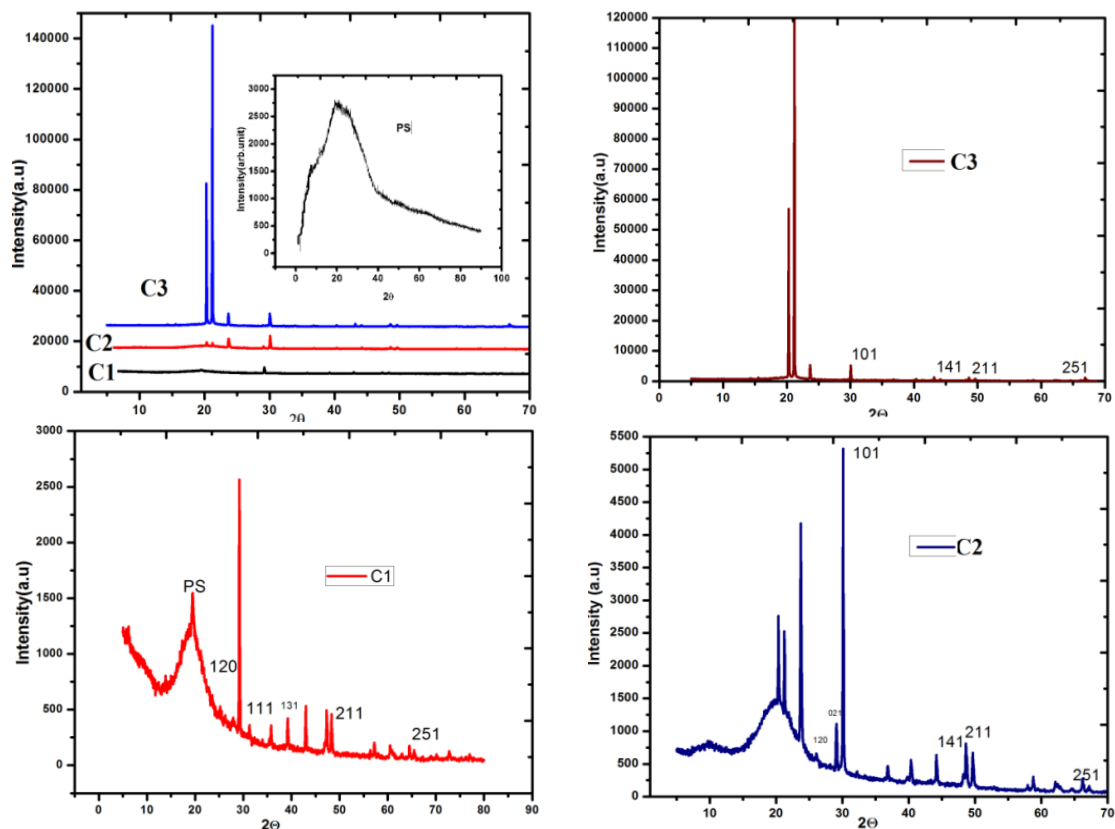
Fig. 1a. X-ray diffractograms Sn: S /PS polynanocmposites ratios (Various Sn: S ratios C1, C2 and C3.
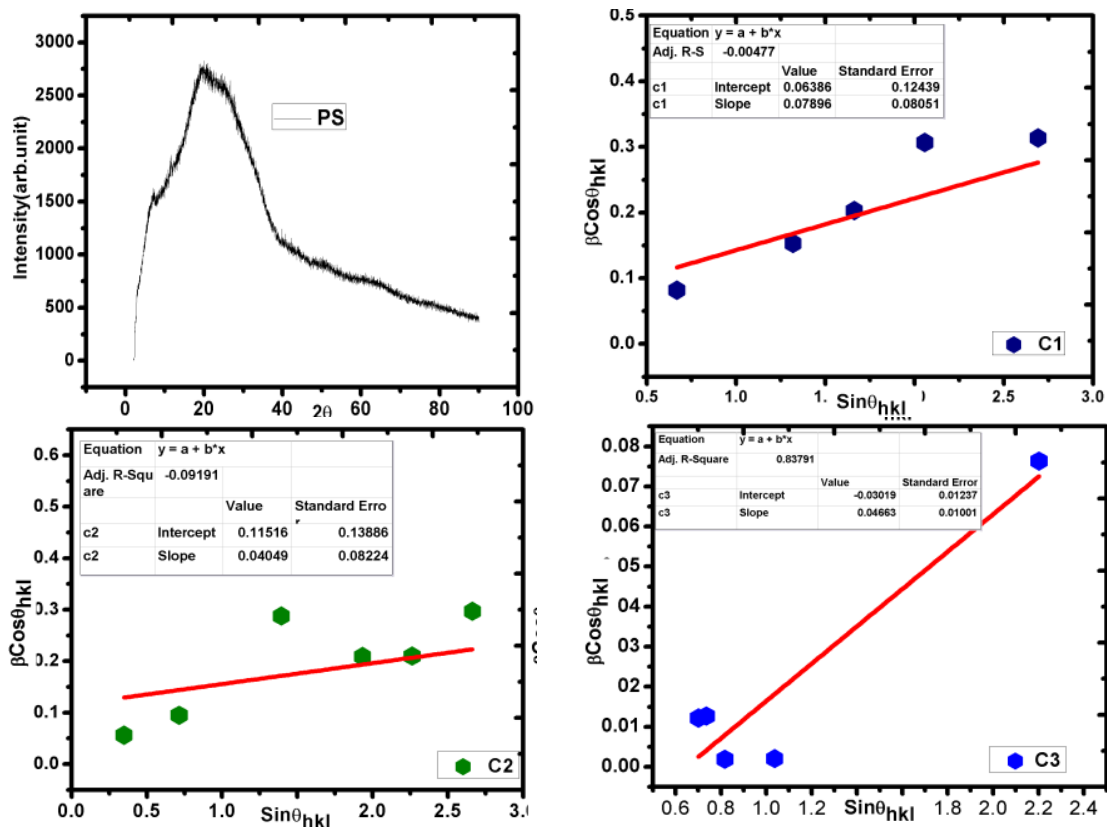
Fig. 1b. William hall plots for Polystyrene SnS_2/PS C1, C2 and C3 samples.

Table 1. Size of samples calculated by Debye Scherer formula and intercept slope by using WHP.

Sample	FWHM	Size (nm)	intercept	Slope
PS	Amorphous only one broad peak			
C1	0.198	9.2	0.06386	0.07896
C2	0.2	6.49	0.115	0.04049
C3	0.024	7.82	-0.030	0.0466

3.2. AFM Morphological studies

AFM micrographs shows in Figure 2a, smooth surface in PS and as the ratio of thiourea increases in SnS_2/PS nanocomposites the spherical shaped particles arranged in regular way on PS surface. In sample C3- the number of spheres increases as shown in Figure2b. According to table 2 the roughness of composites is increases as the SnS nanoparticles increase in PS solution, the roughness confirms that the large and high intensity peaks are obtained in sample C3 than C2 and C1in XRD results. The SnS/PS - C3 shows high crystalinity nature.
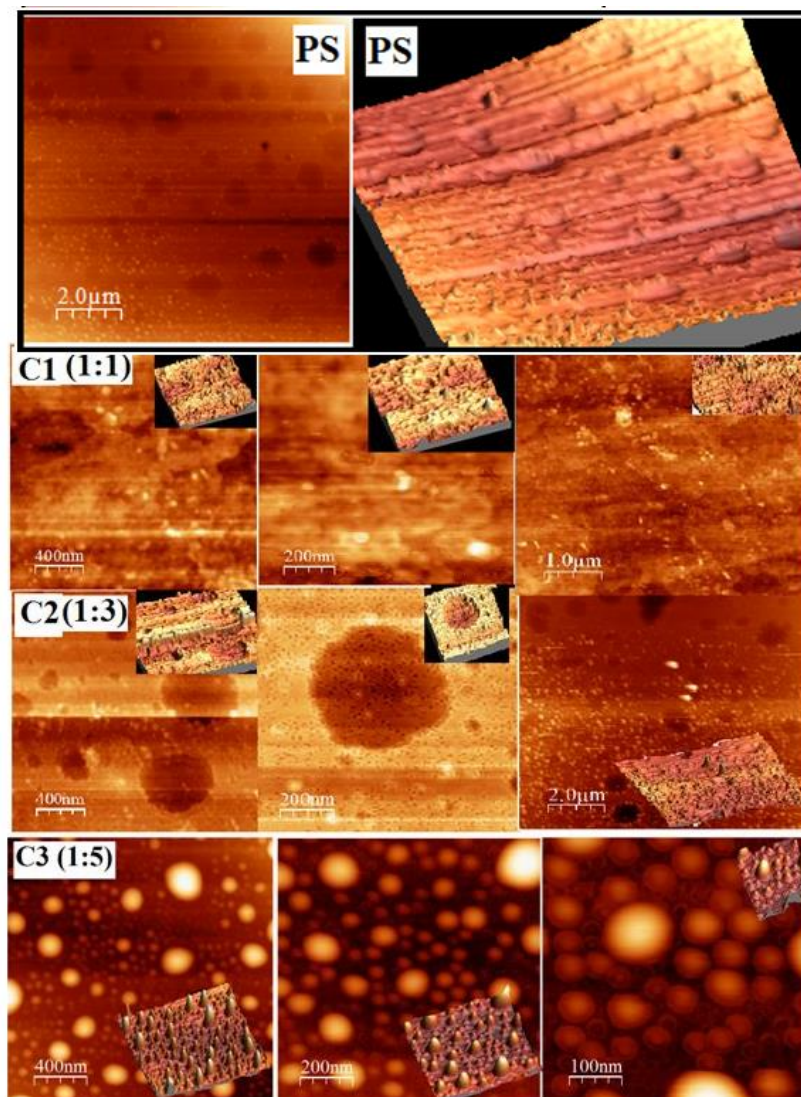
Fig. 2a . AFM Micrographs of SnS/PS polynanocomposites of sample (a) C1 (b) C2 and (c) C3.
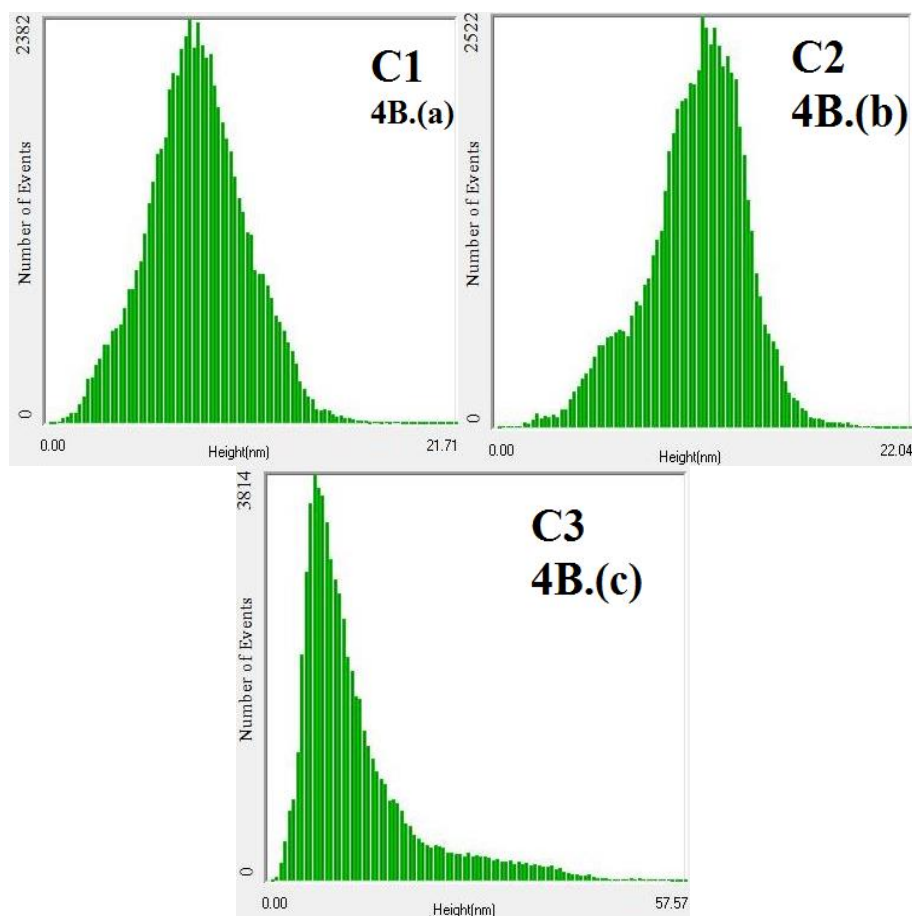
Fig. 2b. Histogram height of particles with AFM Micrographs of SnS/PS polynanocomposites of sample (a) C1 (b) C2 and (c) C3.

Table 2. Roughness and surface kurtosis and skewness calculated by WXSM.

Samples	C1 (1:1)			C2(1:3)			C3(1:5)		
Scale	**400nm**	**200nm**	**1.0um**	**400nm**	**200nm**	**2.0um**	**400nm**	**200nm**	**100nm**
RMS roughness	2.01	2.05	2.46	2.71	1.85	11.4	8.90	1.07	4.2236
Average roughness	1.60	1.60	1.9	2.10	1.41	8.79	6.411	0.167	2.75
Surface skewness	0.64	0.207	0.49	-0.439	-0.32	1.15	1.817	0.94	2.72
Surface kurtosis	4.79	3.54	4.18	3.578	3.63	5.75	6.81	3.68	11.76

3.2.1. Skewness and Kurtosis Measurements (Test)

R_a is roughness parameter, and R_a parameter is same for two different surfaces. In Figure 2b. Histogram shows the roughness and kurtosis and skewness values. This histogram shows the orientation of SnS nanoparticles in the PS. All the average kurtosis and skewness across the SnS orientation were analyzed and shown in Table 2. The orientation of SnS nanoparticles is depends upon the angles and different angles have different values of skewness and kurtosis. The positive skewness value shows smooth surfaces and less roughness. On the other hand if skewness value is negative then it shows more number of deep voids, cracks. This also described that material is

chunks and torn. Materials add in the PS and pull out from that part which is called pitting. Angle 45and 90 orientations of materials show the positive skewness .this means lack of void and cracks on the surface. At 90^0 the kurtosis value is large and this shows the steak and sharp peaks and also lack of tails in negative and positive directions [31]. The carrier concentration increased as the processing temperature decreases in conduction of mechanism the film exhibit a lot of Sulfur vacancies. These SnS nanoparticles were more closely packed in PS as shown in AFM micrographs.

3.3 Optical studies
3.3.1 UV- visible studies

The absorption spectrum of all samples C1, C2, and C3 are measured by UV-visible spectroscopy is shown in Figure 3. All samples displayed optical absorption over the whole visible light spectrum (400–700 nm). The broad spectrum impedance implies that the synthesized SnS_2 hexagonal plates should be an excellent visible light responsive photocatalyst for water and CO_2 splitting. With the increase of sulfur the absorption curves of C2 and sample C3 were shifted towards shorter wavelengths. The bandgap PS were determined with the help of equation 1, the optical absorption is used for direct band gap semiconductors [32]:

$$\alpha h v = \beta \ (hv - \text{Eg}) \ 1/2 \ldots\ldots\ldots\text{.eq [1]}$$

The curves of $(\alpha h v)^2$ versus (hv) for the synthesized PS/ SnS_2 hexagonal were plotted. Generally the band gap PS of SnS2 and SnS are 2.2 and 1.08eV [33]. However, the absorption in the visible region was attributed to the transition from the ground state to a few defect related deep states.
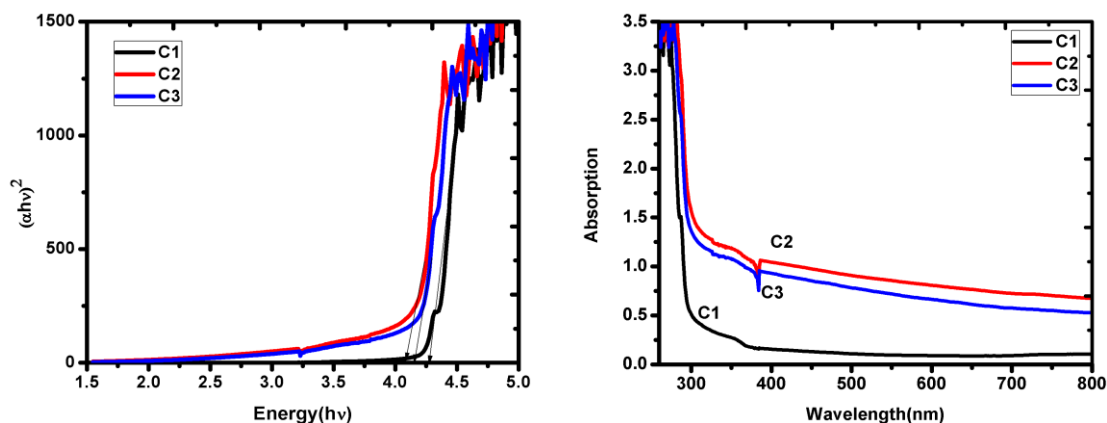
Fig. 3. Optical Spectra of SnS nanoparticles for Sn: S ratios C1 (1:1), C2 (1:3) and C3 (1:5).

3.3.2. Photoluminescence (PL) spectroscopy

Photoluminescence (PL) spectroscopy of sample C1, C2, C3 is shown in Figure6. PL measures the band gap of SnS /PS films and measure the spectrum emitted by the recombination of photogene-rated holes and electrons. On doping of any materials in the semiconductor then it induces the large charge carriers in the band. Figure 4 shows the PL spectra of SnS_2 of three samples of various ratios of thiourea at room temperature. The spectra exhibited a strong emission peak at 350 to 550nm corresponding to green emission. The strong PL peaks might be related to crystalline defects induced during growth. SnS_2 exhibits a luminescence peak for near band emission at 400nm to 550 nm and also exhibits small peaks at 700nm .Typically, a smaller PL intensity indicates better photo activity [33-34]. The intensities of peaks increase on the addition of sulfur quantity in the sample. The broad peak from 400nm to 550nm shows good photoluminescence behavior. And nanoparticles shows blue shift and small peal also absorbed at higher wavelength [35-36]. The composite shows good luminescence in visible light.
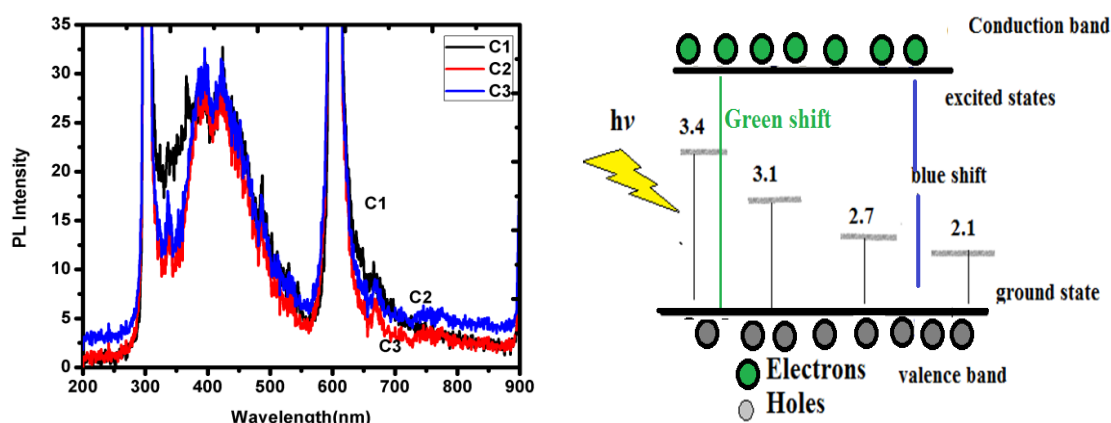
Fig. 4. Optical Spectra of SnS nanoparticles for various Sn: S ratios C1 (1:1), C2 (1:3) and C3 (1:5).

3.4. FTIR Studies

FTIR transmission spectra of SnS particles obtained by SnS/PS ratio 1:1 and 1:5 is shown in Figure 5. The peaks of all samples are calculated in table3. From this spectrum, it can be seen the appearance of bands at 530-560 cm^{-1}, 1400cm^{-1}, 1678cm^{-1} and 2800-3200 cm^{-1}. Strong and broad peaks appear in the spectrum at 560cm^{-1} and 1400 cm^{-1} which are due to the characteristics of SnS. These bands are similar in positions, if compared with others. The band at 1678cm^{-1} is assigned to H-O-H bending of H_2O molecules. Broad band appeared in the range 2800-3200 cm^{-1} is assigned to stretching vibrations of O-H band from hydroxyl group PS or absorbed water present on SnS surface. Characteristic peaks of SnS in FTIR analysis are supported by XRD result and they confirmed the presence of SnS films. The peaks become sharper for higher Sn: S ratio.
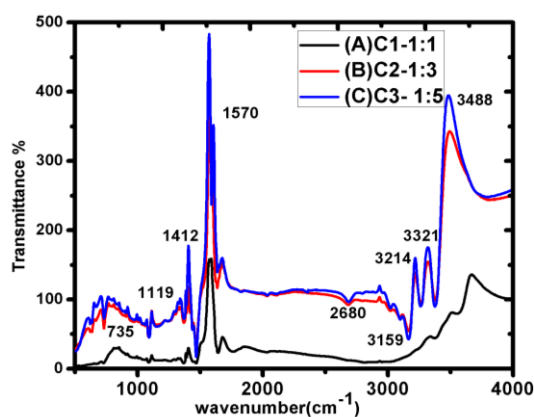
Fig. 5. FTIR Spectra of Sample (A) C1- 1:1(B) C2- 1:3, and (C) C3- 1:5.

Table 3. FTIR attributed peaks of Sample (A) C1- 1:1(B) C2- 1:3, and (C) C3- 1:5.

C1 SnS/PS-1:1		C2 SnS/PS-1:3		C3 SnS/PS-1:5		Streching,Bending vibrations
peaks	Intensity	Peaks	Intensity	Peaks	Intensity	
836	34.3	483,735,907,1119	35,46,90,87	493,728,1090	254,61.1,38	SnS stretching
1404	29.26	1405	115	1412	177	-C=O
1579	154.4	1568	354	1570	461	-NH,-CH$_2$
1687	45.59	1682	162.3	1677	177	C=O
1853	37.43	3158	48	3214	167	
3655	141.69	3207,3314,3501	145,164,341	3488	393	-OH

3.5. Photo catalytic activity

The photocatalytic activities were carried on methyl Red dye with the present of SnS/PS transparent films of different ratios of SnS ratios. The rate of concentration of methyl red is decreases as the illuminations of sunlight time are increases. Concentration of dye fast decreases in sample third C3 than other sample C1 and C2. The absorption curves of methyl Red with the present of samples C1, C2 and C3 shown in figure(6), which shows that how color of dye decreases by photocatalyst and sunlight as the time of illuminations of sunlight increases then the concentration decrease. Max absorption of methyl red dye is 2.4 and as the photocatalyst mix in dye solution then the absorption of dye decreases as shown in figure and reaches zero with in time 90min the c/c_0 vs. time graph in fig shows the decreases of concentration with the photocatalyst, the sample C3 is good sample in which dye decreases fast as comparison to others.
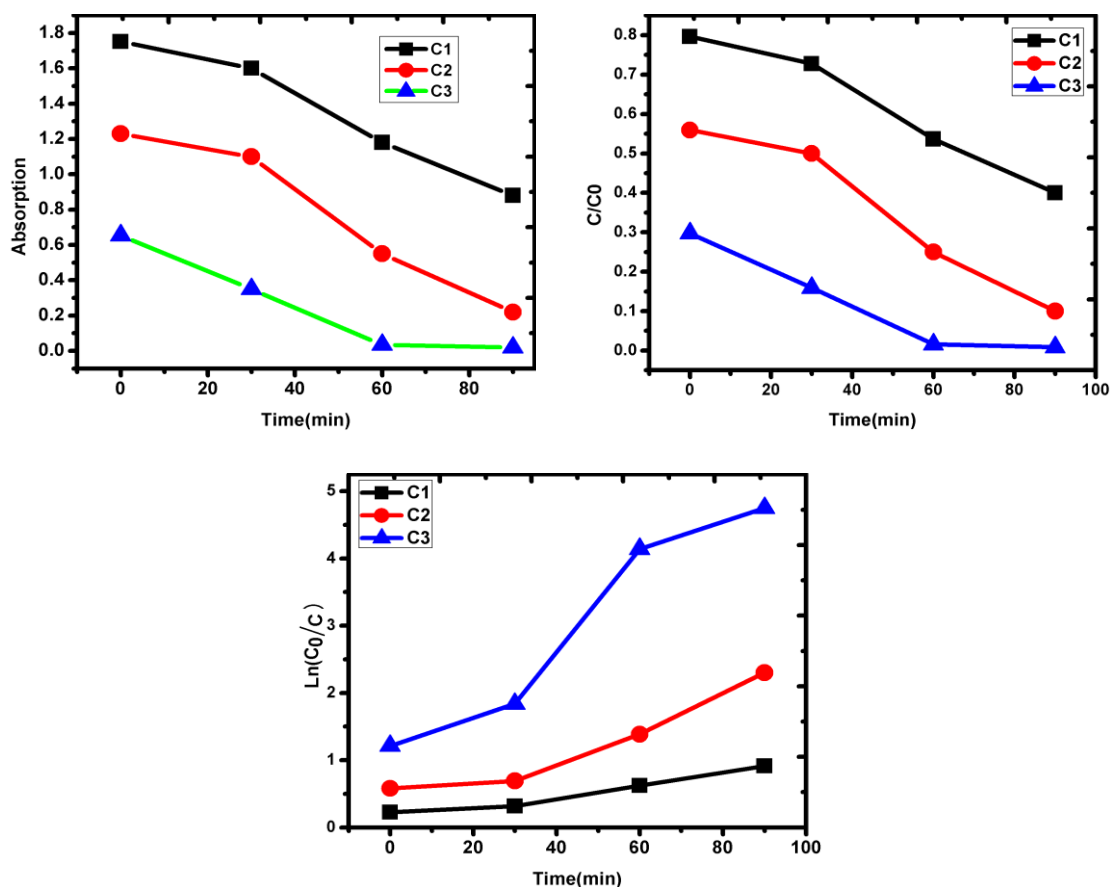
Fig. 6. Desorption curves of methyl red dye with the presence of sunlight and photocatalyst.

3.5.1 Photocatalytic degradation

The degradation percentage of methyl red by SnS/PS nanocomposite and films were calculated by using equation

$$\text{Degradation percentage-} = (\frac{A0-A}{A0})\text{x } 100\%$$

where A_0 is concentration of dye solution at time zero and A is the concentration of dye solution at time t.the calculated percentage is given in table according to percentage C3 sample is good efficiency than others for example the third sample C3 has 97% degradation rate due to higher and lower in C2 - 82.1% and C1- 49.7%. The histogram in Figure 7 shows the percentage of degradation.
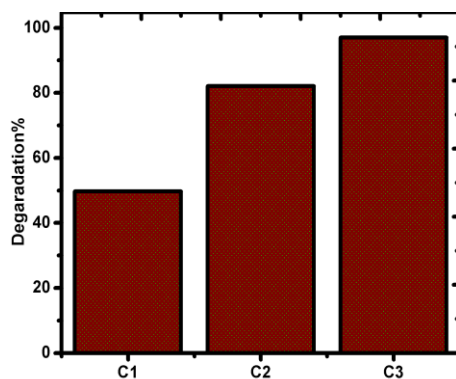
Fig. 7. Histogram of percentage degradation of methyl red dye.

3.5.2. Kinetic behavior of photocatalytic

The kinetic behavior of photocatalytic Langmuir Hinshelwood kinetic equation is used to determine the behavior of reaction and linear fitting of curve shows the pseudo first order reaction. The rate of constant k increases in sample C3. And rate of reaction is slow in sample C2 and C1. As shown in Figure11.
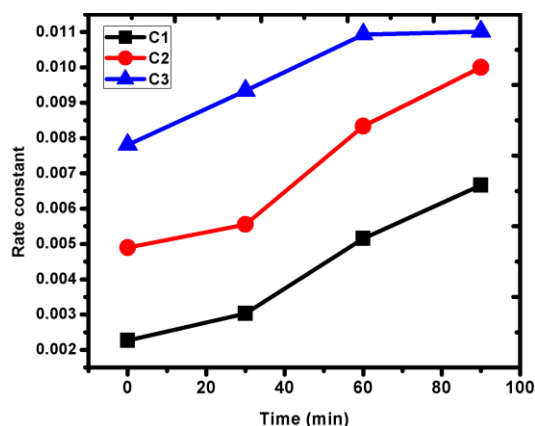
Fig. 11. Rate constant k of degradation of methyl red.

Table 4. Percentage and rate constant of degradation of dyes.

Sample Code	Degradation %	Rate Constant
C1	49.7	0.004278
C2	82.1	0.007197
C3	97	0.009775

3.5.3. Mechanism

The mechanism of photocatalytic splitting electrons and holes in the presence of sunlight. The photocatalyst has four steps.

1. Light harvesting
2. Charge excitation
3. Charge separation
4. Transfer
5. Surface catalytic reactions or Redox reaction.

When photocatalyst is exposed to sunlight then due to light it acquired sufficient amount of photons and electrons of SnS/PS nanocomposite film excited from valence band to conduction band and holes are remaining in the valence band. The electrons and holes are involved in redox reaction with water. The photo-excited electrons react with oxygen and generates superoxide ions which further react with hydrogen and produced OH* radicals which react with dyes molecules and degraded into CO_2 and H_2O.
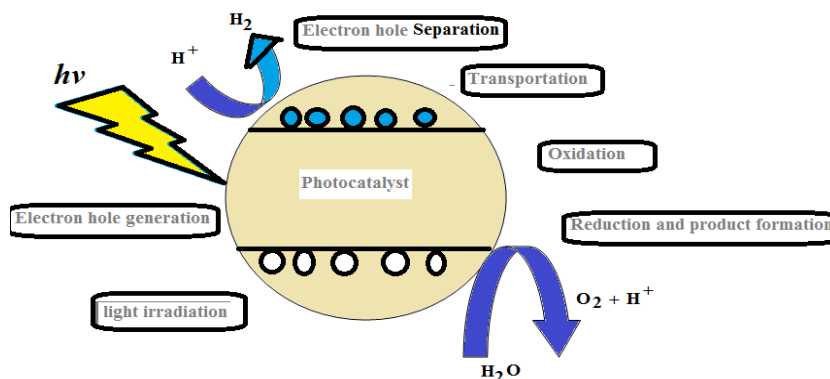
Fig. 12. Schematic diagram of photocatalyst.

4. Conclusions

SnS Nanoparticles were synthesized using low cost sol gel route. Various ratios of Sn and S have been analyzed. The obtained samples were analyzed by structural, optical, Photoluminescence and FTIR studies. An XRD spectrum shows hexagonal SnS_2 structures. On increasing the thiourea improves the Crystalline. Excellent optical and PL properties make them suitable for optoelectronic applications. The band gap of the samples are about 2.5eV that also confirms the existence of SnS_2 form Samples also exhibit excellent photoluminescence behaviour. PL spectra shows peaks at 393nm and 450 nm and the intensity of the peaks increase with in molar ratio of the Sn and S in the starting solution. Strong and broad peaks appear in the spectrums at 550 and 1400cm -1 which are due to the characteristics of SnS. Characteristic peaks of SnS in FTIR analysis are supported by XRD result and they confirmed the presence of SnS films. The peaks become sharper for higher Sn: S ratio. The transmission of PS is decreases and resistivity increases as the SnS increases in the PS films. The flexible films are conducting and transparent. In photocatalytic activity 97% degradation occurs.

References

[1] M. A. Green, J Mater Sci: Mater. Electron. 18 (2007) S15-S19; https://doi.org/10.1007/s10854-007-9177-9

[2]. Lee, D.; Yong, K.. Korean J. Chem. Eng. 2013, 30, 1347-1358; https://doi.org/10.1007/s11814-013-0101-0

[3]. Y. Lee, Y. Lo,. Adv. Funct. Mater. 19,604-609 (2009); https://doi.org/10.1002/adfm.200800940

[4]. Lim, E.; Chun, J.; Jo, C.; Hwang, J.. Korean J. Chem. Eng. 2021, 37, 1-21;

[5] Ranjana Sharma, Vijay Kumar and Y C Goswami, Chalcogenide letters 18 (8) (2021), 473-479.

[6] R Bisauriya, Saurabh Khandelwal and Y C Goswami, Material today proceedings 47 (18), 2021, 6379-638.

[7] UPS Gahlaut, V Kumar, YC Goswami, Physica E: Low-dimensional Systems and Nanostructures 117, 113792;

[8] J. B. Johnson, H. Jones, B. S. Latham, J. D. Parker, R. D. Engelken, C. Barber, Semicond. Sci. Technol. 14 (1999) 501; https://doi.org/10.1088/0268-1242/14/6/303

[9]. W. Wang, L. Shi, D. Lan, Q. Li, J.Power Sources 377, 1-6 (2018); https://doi.org/10.1016/j.jpowsour.2017.11.084

[10]. F.W. Lee, C.W. Ma, Y.H. Lin, P.C. Huang, Y.L. Su, Y.J. Yang, Sens. Mater. 28, 7 (2016).

[11]. Abdelbasir, S.M.; Shalan, A.E., Korean J. Chem. Eng. 2019, 36, 1209-1225; https://doi.org/10.1007/s11814-019-0306-y

[12] Adhikari, S.; Mandai, S.; Kim, D.-H., Korean J. Chem. Eng. 2020, 37, 2359-2367; https://doi.org/10.1007/s11814-020-0705-0

[13]. C. Lai, M. Lu, L. Chen, J.Mater. Chem. 22, 19-30 (2012); https://doi.org/10.1039/C1JM13879K

[14] A. Muthuvinayagam, B. Viswanathan, Indian J. Chem.Sect. A 54, 155-160 (2015)

[15] M.Saleem, G. Mehboob, M. Shafiq Ahmed, Said Nasir Khisro,M. Z. Ansar , Kashif Mehmood, Rafiqa-Tul-Rasool , M. K. Alamgir , Ahsan Ejaz ,M. Ghazanfar , Shahnwaz Hussain, Adil Ahmed and J. M. Ashfaq, Frontiers in Chemistry, 8, (2020), DOI https://doi.org/10.3389/fchem.2020.00254

[16] A. Muthuvinayagam, B. Viswanathan, Hydrothermal synthesis and LPG sensing ability of SnS nanomaterial. Indian J. Chem.Sect. A 54, 155-160 (2015)

[17] J. Henry, K. Mohanraj, S. Kannan, S. Barathan, G. Sivakumar, J. Exp. Nanosci. 10 (2015) 78-85; https://doi.org/10.1080/17458080.2013.788226

[18] P. K. Duttaand S. Mitra Materials Today: Proceedings Polystyrene : synthesis, characteristics, and applications / editor, Col5 (2018) 23321-23325

[19] Lynwood,http://www.novapublishers.com. TP1180.S7P665 2014,668.4'233--dc23; https://doi.org/10.1016/j.matpr.2018.11.067

[20] Ruziwa, D., Chaukura, N., Gwenzi, W., Pumure, I, J. Environ. Chem. Eng. 3(2015) 2528-2537; https://doi.org/10.1016/j.jece.2015.08.006

[21] Geovania C. de Assis, Euzébio Skovroinski,Valderi D. Leite,Marcelo O. Rodrigues,André Galembeck,Mary C.F. Alves, Julian Eastoe, and Rodrigo J. de Oliveira, , ACS Appl. Mater. Interfaces 10 (2018) 8077−8085; https://doi.org/10.1021/acsami.7b19834

[22] Jui Hung Chen and Chu-Yun Cheng, European Polymer Journal 44 (2008) 3271-3279; https://doi.org/10.1016/j.eurpolymj.2008.07.023

[23] S. M. Ahamed, A. A. A. Darwish, E. A. El-Sabagh, N. A. Mansour, D. E. Abulyazied, E. S. Ali, Journal of Ovonic Research, 16(1) p. 71 – 81 (2020).

[24] Dong Wook Chae and Byoung Chul Kim, Polymers for advanced technologies, Division of Applied Chemical & Bio-engineering, 133-791, (2005).

[25] C. Saujanya and S. Radhakrishnan, Polymer, pp. 6723-6731, (2001) https://doi.org/10.1016/S0032-3861(01)00140-9

[26] H. Huang, Zhang and J. J, Journal of Applied Polymer Science, vol. 111, pp. 2806-2812, 2009; https://doi.org/10.1002/app.29336

[27] J. R. Brent, D. J. Lewis, T. Lorenz, E. A. Lewis, N. Savjani, S. J. Haigh, G. Seifert, B. Derby and P. O'Brien, J. Am. Chem. Soc., 2015, 137, 12689-12696; https://doi.org/10.1021/jacs.5b08236

[28] He, M.; Yuan, L.-X.; Huang, Y.-H., RSC Adv. 2013, 3, 3374-3383; https://doi.org/10.1039/c2ra22764a

[29] Wei, R.; Zhou, T.; Hu, J.; Li, J., Mater. Res. Express 2014, 1, 025018; https://doi.org/10.1088/2053-1591/1/2/025018

[30] Yao, K.; Li, J.; Shan, S.; Jia, Q., Catal. Commun. 2017, 101, 51-56; https://doi.org/10.1016/j.catcom.2017.07.019

[31] B.D. Cullity & S.R. Stock, 2001, p 167-171.

[32] Prabhu, Y.T., Rao, K.V., Kumar, V.S.S. and Kumari, B.S. (2014). World Journal of Nano Science and Engineering, 4, 21-28.http://dx.doi.org/10.4236/wjnse.2014.41004; https://doi.org/10.4236/wjnse.2014.41004

[33] N Duboust, H Ghadbeigi , C Pinna , S Ayvar-Soberanis , A Collis , R Scaife and K Kerrigan, Journal of Composite Materials 2017, Vol. 51(3) 289-302, DOI: 10.1177/0021998316644849; https://doi.org/10.1177/0021998316644849

[34] B. Liu, X. Zhao, Q. Zhao, X. He, and J. Feng, Journal of Electron Spectroscopy and Related Phenomena, vol. 148, no. 3, pp. 158-163, 2005; https://doi.org/10.1016/j.elspec.2005.05.003

[35] Guo Yuying, Shi Weimin, Wei Guangpu,Thin Solid Films, 2002, 403 -404: 116-119; https://doi.org/10.1016/S0040-6090(01)01520-6

[36] K.T.Ramakrishna Reddy, P.Purandhara Reddy, P.K.Datta,et al., Thin Solid Films, 2002, 403 - 404: 116-119; https://doi.org/10.1016/S0040-6090(01)01520-6